

Lattice QCD on nonorientable manifoldsSimon Mages,^{1,2,*} Bálint C. Tóth,^{3,†} Szabolcs Borsányi,³ Zoltán Fodor,^{1,3,4}
Sándor D. Katz,⁴ and Kálmán K. Szabó^{1,3,‡}¹*Jülich Supercomputing Center, Jülich D-52425, Germany*²*University of Regensburg, Regensburg D-93053, Germany*³*University of Wuppertal, Department of Physics, Wuppertal D-42097, Germany*⁴*Eötvös University, Budapest 1117, Hungary*

(Received 27 January 2016; published 30 May 2017)

A common problem in lattice QCD simulations on the torus is the extremely long autocorrelation time of the topological charge when one approaches the continuum limit. The reason is the suppressed tunneling between topological sectors. The problem can be circumvented by replacing the torus with a different manifold, so that the connectivity of the configuration space is changed. This can be achieved by using open boundary conditions on the fields, as proposed earlier. It has the side effect of breaking translational invariance strongly. Here we propose to use a nonorientable manifold and show how to define and simulate lattice QCD on it. We demonstrate in quenched simulations that this leads to a drastic reduction of the autocorrelation time. A feature of the new proposal is that translational invariance is preserved up to exponentially small corrections. A Dirac fermion on a nonorientable manifold poses a challenge to numerical simulations: the fermion determinant becomes complex. We propose two approaches to circumvent this problem.

DOI: [10.1103/PhysRevD.95.094512](https://doi.org/10.1103/PhysRevD.95.094512)**I. INTRODUCTION**

Lattice regularization is a powerful method to carry out calculations in a quantum field theory. It provides a well-defined, systematically improvable framework, which also works in the nonperturbative regimes of the theory. There is currently a lot of activity to calculate various observables in Quantum Chromodynamics (QCD) by carrying out numerical computations on lattices. Such activities are an important cornerstone in the search for physics beyond the Standard Model. In many cases lattice results with a precision beyond the % level are needed to fully exploit the discovery potential of these searches. To reach such a precision it is important to have a reliable error estimation.

One type of error comes from the autocorrelation in the Monte Carlo time series of the numerical simulations. In principle, one has to run the simulation several times longer than the largest autocorrelation time in the system. Typically the slowest modes correspond to observables which are related to the topology of the field space, like the topological charge

$$Q = \int_{\mathcal{M}} d^4x q(x), \quad (1)$$

where $q(x) = \frac{1}{32\pi^2} \epsilon_{\mu\nu\rho\sigma} \text{tr} F_{\mu\nu} F_{\rho\sigma}$ is the topological charge density. In practice, the space-time manifold \mathcal{M} is chosen to be the torus, where periodic/antiperiodic boundary

conditions are imposed on the fields. On the torus Q is quantized, and the field space splits into disconnected sectors labeled by integer [1] values of Q . The advantage of the torus is translational invariance, and as a consequence the results have small finite volume corrections. The disadvantage is that conventional simulation algorithms have severe difficulties changing the topological properties of the field configurations, and it gets worse with decreasing lattice spacing. The autocorrelation time of the topological charge was found to increase with the sixth power of the inverse lattice spacing in actual simulations [2]. Rare tunneling events make the extraction of the topological susceptibility challenging. For a recent proposal see [3]. Besides the susceptibility, the accurate computation of observables that correlate strongly with topology is also challenging.

The slow modes can be removed from the theory by changing the topology of the manifold \mathcal{M} . The authors of [4] proposed to introduce an open boundary in one of the directions. This change in the topology of space-time also changes the topology of the gauge field configuration space, which becomes connected and Q is not restricted to an integer value anymore. This eliminates the slow modes from the theory. Indeed, in [4] a drastic reduction of the autocorrelation time of the topological charge was observed. A disadvantage of this approach is the lack of the translational invariance in the open direction, which introduces boundary effects and decreases the effectively available space-time volume. There are several recent studies with open boundary conditions, which address the systematics of the method [5–8].

*simon-wolfgang.mages@ur.de

†tothbalint@szofi.elte.hu

‡szaboka@general.elte.hu

where a particle propagates around the t direction. Therefore, they have to be exponentially suppressed with T times the massgap of the theory.

The P -periodic boundary condition is similar to the C -periodic boundary condition of Refs. [18–20], where a charge conjugation is performed when the boundary is crossed. They lead to processes which change the total electric charge: charge fluctuations when propagating through the C -periodic boundary change their sign and thereby the total electric charge. Analogously, our P -periodic boundary condition leads to changes in the total topological charge. Also, just as in the C -periodic case, the ultraviolet structure of the theory is not affected by the boundary condition and the same renormalization applies as in infinite volume [20].

The implementation of the parity transformation on parallel computers can be cumbersome. Therefore, we choose another transformation, which serves the purpose equally well: the lattice points shall be reflected through the $x = 0$ hyperplane. Since this transformation is a product of P and a rotation by 180° around the x axis, it also changes the orientation and defines a nonorientable manifold. For simplicity we use the name “ P -periodic” boundary condition for this setup in the rest of the paper.

III. GAUGE FIELDS

To demonstrate the viability of our proposal, we performed numerical simulations in pure SU(3) gauge theory. The prescription for the P boundary is

$$\begin{aligned} U_x(x, y, z, t + T) &= U_x^\dagger(L - x - 1, y, z, t), \\ U_i(x, y, z, t + T) &= U_i(L - x, y, z, t) \end{aligned} \quad (3)$$

for $i = y, z, t$. In the other three directions we keep the usual periodic boundary condition. We use the tree-level Symanzik-improved action [21] and lattices of a fixed physical size of $L = T \sim 2.27/T_c$. One update sweep consists of four overrelaxation and one heatbath steps [22–24]. There is practically no overhead on the simulation time coming from the P -boundary condition. We chose five different lattice spacings. The lattice size, gauge coupling, w_0 scale [25], the lattice spacing, and the number of update sweeps are given in Table I. The lattice spacings shown are obtained from the conversion $a = 0.167 \text{ fm}/w_0$ [26]. For comparison we simulate three streams at every set of parameters: one with periodic, one with open, and one with P -periodic boundaries. Our main observables are the topological charge Q and time slice averages of the topological charge and action densities $Q(t)$ and $E(t)$ as defined in [4]. All are evaluated along the Wilson flow [27] at a flow time of w_0^2 .

Figure 2 shows the simulation time history of the topological charge for the finest lattice spacing. It already shows a drastic reduction of the autocorrelation of Q .

TABLE I. Lattice Parameters

L	β	w_0	a [fm]	n_{sweep}
16	4.42466	1.79	0.093	2×4001
20	4.57857	2.24	0.075	3×4001
24	4.70965	2.65	0.063	4×4001
32	4.92555	3.43	0.049	10×4001
40	5.1	4.13	0.040	19×4001

The discrete nature of the topological charge in the periodic case can be seen best in a histogram of the topological charge, which is given in Fig. 3 together with the histograms of the charges with the other two boundary conditions, which show no sign of discretization.

The lattice spacing dependence of the integrated autocorrelation time of the topological charge $\tau_{\text{int}}(Q)$ is given in Fig. 4. Again, one can clearly see that both open and P -periodic boundaries give a strong reduction of $\tau_{\text{int}}(Q)$ compared to the periodic case. Though P -periodic simulations have somewhat larger autocorrelation times than the open simulations, they seem to scale with a similar power of the lattice spacing.

In [28] a simple model was set up to describe the scaling of $\tau_{\text{int}}(Q)$ with the lattice spacing. There the autocorrelation function of the topological charge is investigated: $\Gamma(t, \tau) = \langle Q(t)_\tau Q(0)_0 \rangle$, where $Q(t)_\tau$ is the time-slice topological charge after τ update sweeps. A diffusion equation for Γ is set up, whose solutions describe numerical data from periodic and open lattices quite accurately. The extremely large autocorrelation times of the topological charge on periodic lattices are attributed to the presence of zero

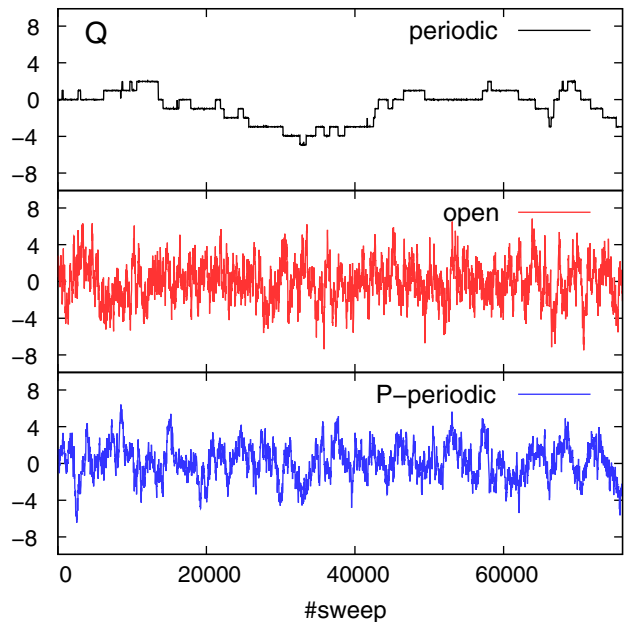


FIG. 2. History of the topological charge Q at $\beta = 5.1$. The corresponding lattice spacing is 0.040 fm.

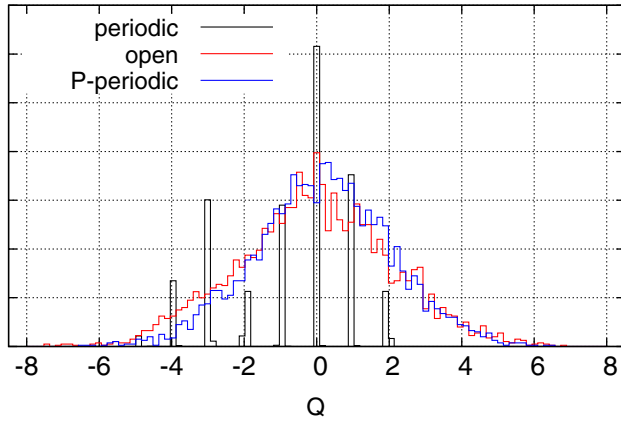


FIG. 3. Histogram of the topological charge Q at $\beta = 5.1$. The corresponding lattice spacing is 0.040 fm.

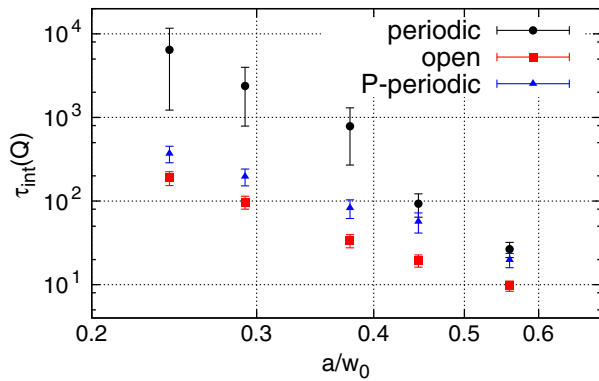


FIG. 4. Integrated autocorrelation time of the topological charge as a function of the lattice spacing.

timelike momentum modes in Γ . They arise due to the periodicity of Γ in the t variable: $\Gamma(t+T, \tau) = \Gamma(t, \tau)$, which is the consequence of the periodic boundary $Q(t+T) = Q(t)$. These zero modes are shown to be eliminated by changing the boundary condition from periodic to open [28]. Repeating the calculation for the P boundary, we see that the same elimination occurs. The zero modes are absent since, as explained before, the charge is antiperiodic $Q(t+T) = -Q(t)$, and therefore Γ is also antiperiodic: $\Gamma(t+T, \tau) = -\Gamma(t, \tau)$. Without these zero modes the autocorrelation time of Q scales similarly to that of the local observables. Let us note that the diffusion and local tunneling parameters of this model do not depend on the boundary condition. Our findings are in agreement with the qualitative picture taken from this model calculation.

Now we come to the most important feature of our proposal. In contrast to the open boundary condition, the P -periodic boundary is translationally invariant in the t direction by construction. This is shown in Figs. 5 and 6. Figure 5 gives the time-slice averaged action $E(t)$ as the function of time. For the usual and P -periodic boundaries $E(t)$ are practically constant and agree well with each other, reflecting translational symmetry and the absence of large

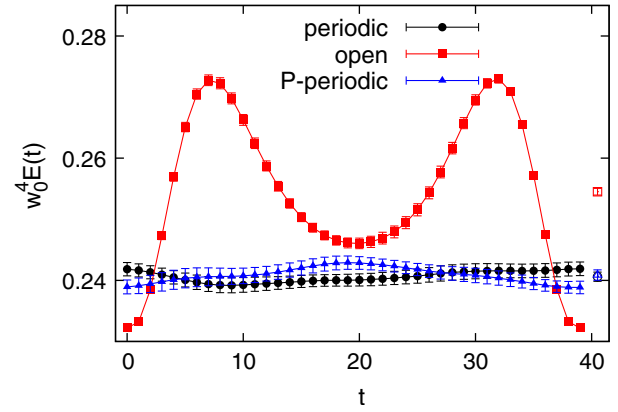


FIG. 5. Time-slice averaged action density at $\beta = 5.1$, lattice spacing $a = 0.040$ fm, and box size 1.6 fm. Filled symbols give the per time-slice results, while open symbols give the result for the full volume.

finite volume effects. The open boundary result deviates from them significantly. Although it is expected to approach the periodic value in the middle of the lattice, here the time extent was not large enough to reach it.

Similar effects can also be seen in Fig. 6, which gives the integrated autocorrelation time of the topological charge on a time slice as a function of time. Again the results for periodic and P -periodic boundaries are independent of time, while the result for open boundaries has a dependence on the distance from the boundary. Additionally, this plot shows that compared to the full volume results the integrated autocorrelation time of the topological charge on a single time slice improves for all choices of the boundary. In the periodic case, however, the result for a single time slice is larger than the result for open and P -periodic boundaries. The reasoning of the subvolume method [3] would suggest that the autocorrelation time on the smallest subvolume—a single time slice—would be the

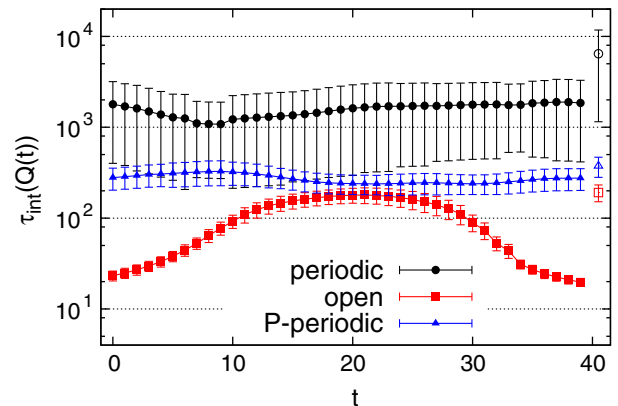


FIG. 6. Integrated autocorrelation time of the topological charge on a time slice at $\beta = 5.1$, lattice spacing $a = 0.040$ fm, and box size 1.6 fm. Filled symbols give the per time-slice results, while open symbols give the result for the full volume.

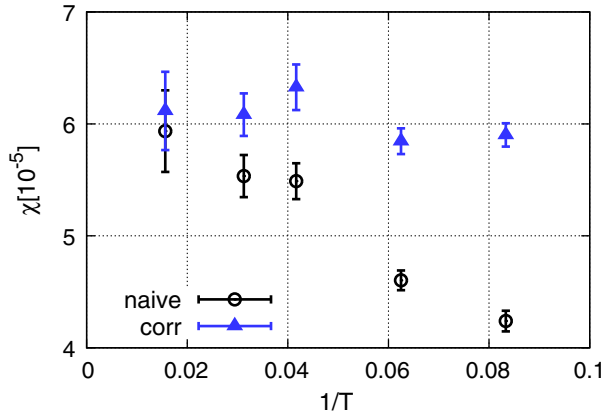


FIG. 7. Finite size dependence of different topological susceptibility definitions for P -periodic boundary conditions at $\beta = 4.42466$, lattice spacing $a = 0.093$ fm.

same independent of the boundary conditions. In the diffusion model one can see why this might be not the case: there is a zero mode contributing to the autocorrelation time only in the periodic case, but not in the open or P -periodic case, which increases the autocorrelation.

The reason for Q being not quantized with P -periodic boundary condition is the lack of translational invariance for Q as described earlier. This demands some additional care when calculating an observable like the topological susceptibility. The appropriate procedure uses the definition via the topological charge density correlator, where we place the origin of the correlator to timeslice $T/2$,

$$\chi = \int_0^T dt \int d^3x \langle q(\vec{x}, t) q(\vec{x}, T/2) \rangle. \quad (4)$$

It has exponentially small finite volume corrections as T is increased since when t in the integral is close to 0 or T , the correlator is exponentially small. Also, this definition is symmetric in t and leads to a maximal cancellation of the negative tail of the correlator with its positive core. To illustrate this, we generated dedicated ensembles at $\beta = 4.42466$ with size $16^3 \times T$ with $T = 12, \dots, 64$. The results show no significant finite volume effects, as shown in Fig. 7 with the label “corr.” The more commonly used definition for the susceptibility is $\langle Q^2 \rangle / (L^3 T)$. For periodic boundary condition the two definitions are equivalent due to the translational invariance. In the P -periodic case the latter definition gives an observable that has finite size effects proportional to $1/T$; see the points with the label “naive” in Figure 7. Let us remark that a similar prescription as in Eq. (4) can also improve the finite volume correction of the standard subvolume method in periodic simulations.

IV. FERMIONS

While nonorientability can be implemented on the gauge fields right away, it becomes nontrivial for fermions. As the boundary mixes the handedness, it is not possible to define

Weyl fermions on a nonorientable manifold. The definition of Dirac fermions is straightforward [29]; the fields undergo an x -axis reflection on the boundary. However, we encounter a serious obstacle: the Dirac matrix entering in the x -axis reflection ($\gamma_5 \gamma_x$) spoils the γ_5 Hermiticity of the Dirac operator and leads to a complex fermion path integral. Numerical simulations with standard algorithms are not possible in this case. Here we show two workarounds.

The first solution is to combine the x reflection with a charge conjugation. Since the topological charge is not only P -odd but also CP -odd, this combination has the same advantageous effect as the P -periodic boundary condition. Instead of the usual $\psi, \bar{\psi}$ fields, it turns out to be more convenient to work with the eigenstates of charge conjugation. These are the spinor fields η_a , $a = 1, 2$, defined in [20]. In both bases we can write down the one flavor fermion action in infinite volume,

$$S_f = \bar{\psi} D[U] \psi = -\frac{1}{2} \eta_a C \hat{D}[U]_{ab} \eta_b, \quad (5)$$

where D is some possibly massive lattice Dirac operator using the usual symmetric expression for the time derivatives, and C is the charge conjugation matrix. The hatted Dirac operator $\hat{D}[U]$ can be written with the original Dirac operator as $\hat{D}[U]_{ab} = D[\text{Re}U \cdot \delta_{ab} - i \text{Im}U \cdot \rho_{2,ab}]$ with the Pauli matrices ρ_i acting on the a index of the η_a fields. As the map $U \mapsto \text{Re}U \cdot \delta_{ab} - i \text{Im}U \cdot \rho_{2,ab}$ defines a representation of $SU(3)$ equivalent to $\mathbf{3} \oplus \mathbf{3}^*$, Eq. (5) is valid not only for Dirac operators which are linear in the links but also for operators which are linear in products of links, such as the clover-improved Wilson-Dirac operator. Equation (5) is even valid for some more general cases, like the overlap operator. For the readers' convenience we collect the symmetries of S_f in this somewhat uncommon representation in the appendix. Now we introduce the “ CP -boundary” condition

$$\eta(x, y, z, t + T) = -\gamma_5 \gamma_x \rho_2 \rho_3 \eta(L - x, y, z, t), \quad (6)$$

where we used the x reflection and charge conjugation operators defined in the appendix. The gauge fields also have to undergo a CP -transformation; this means additional complex conjugations in Eq. (4). The resulting Dirac operator is $\gamma_5 \rho_2$ Hermitian

$$\hat{D}^\dagger = \gamma_5 \rho_2 \hat{D} \gamma_5 \rho_2 \quad (7)$$

since the matrix $\gamma_5 \rho_2$ commutes with the boundary condition [30]. Therefore, the path integral over the η fields gives a real Pfaffian. In the massless case and in the continuum \hat{D} also satisfies

$$\{\hat{D}, \gamma_5 \rho_2\} = 0 \quad \text{for } m = 0. \quad (8)$$

There is no continuous chiral symmetry behind this relation, but only a discrete one $\eta \rightarrow \gamma_5 \rho_2 \eta$. For further

fermionic symmetries see the appendix. The argument presented in [20] for the case of the C -boundary condition also applies for the CP -boundary: for those symmetries that are broken by the boundary, the breaking is expected to fall off exponentially in T .

Another solution to the complex determinant problem can be given for two degenerate flavors. Then the recipe is to add an extra rotation in flavor space at the boundary as

$$\eta(x, y, z, t + T) = -\gamma_5 \gamma_x \rho_2 \tau_1 \eta(L - x, y, z, t), \quad (9)$$

where τ_i 's are Pauli matrices in flavor space, and now the η carries a flavor index, too. This makes the fermion path integral real since the Dirac operator is $\gamma_5 \tau_3$ Hermitian. This solution can be written in the usual four-component spinor basis, and it can be implemented in a similar way as the so-called G -parity boundary condition [31]. Equation (9) can be also applied to unrooted staggered fermions.

To get the expression for the two point pion correlation function, the interpolating operators are needed in the Majorana basis,

$$\begin{aligned} \mathcal{O}_{\pi^-} &= \bar{\psi}_u \gamma_5 \psi_d = -\frac{1}{2} \eta_u^t \gamma_5 C (1 - \rho_2) \eta_d, \\ \bar{\mathcal{O}}_{\pi^-} &= -\bar{\psi}_d \gamma_5 \psi_u = \frac{1}{2} \eta_d^t \gamma_5 C (1 - \rho_2) \eta_u. \end{aligned} \quad (10)$$

The correlator between x and y then is

$$\begin{aligned} \langle \mathcal{O}_{\pi^-}(x) \bar{\mathcal{O}}_{\pi^-}(y) \rangle \\ = -\frac{1}{4} \langle (\eta_u^t)_x \gamma_5 C (1 - \rho_2) (\eta_d)_x (\eta_d^t)_y \gamma_5 C (1 - \rho_2) (\eta_u)_y \rangle, \end{aligned} \quad (11)$$

which after integrating out the Grassmann fields and choosing $m_u = m_d$ becomes

$$\begin{aligned} \langle \mathcal{O}_{\pi^-}(x) \bar{\mathcal{O}}_{\pi^-}(y) \rangle \\ = \frac{1}{4} \text{Tr} [(\hat{D}^{-1})_{y,x} \rho_2 (\hat{D}^{-1})_{x,y}^\dagger \rho_2 + (\hat{D}^{-1})_{y,x} (\hat{D}^{-1})_{x,y}^\dagger]. \end{aligned} \quad (12)$$

More point correlation functions can be constructed analogously.

As a first exploratory study we implemented the CP -boundary condition with a Wilson-Dirac operator. Quenched configurations were generated with CP boundary and we found that the observables and, in particular, their autocorrelation times were consistent with the respective P -boundary condition values. To study the above proposal for fermions, we took CP -boundary configurations generated at $\beta = 4.35$ on $16^3 \times 32$ lattices, $w_0 = 1.57$. Four steps of stout smearing with smearing parameter 0.125 were applied [32]. The π^+ pion propagator was measured at the bare Wilson mass -0.16 ; see upper panel of Fig. 8.

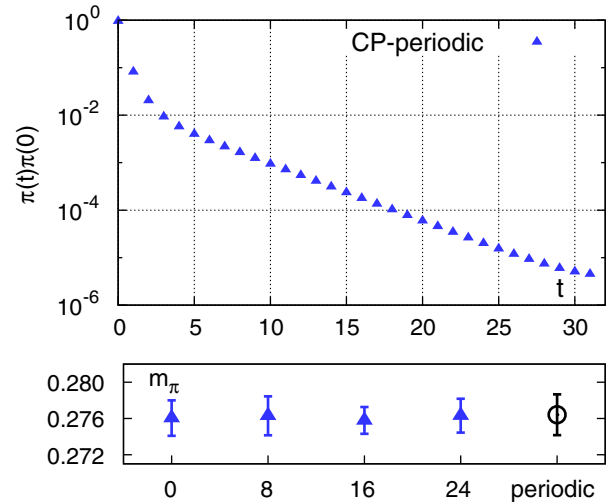


FIG. 8. *Upper*: Pion propagator with CP -boundary condition. *Lower*: Pion masses obtained after shifting the gauge field by 0, 8, 16, and 24 units in t direction (filled), and with periodic boundary condition (open).

Contrary to the usual periodic case, the propagator is a single exponential for times far away from $t = 0$ and T . There is no backward contribution coming from the antiparticle π^- . The reason for this is that the antiparticle π^- is now transformed under CP conjugation to a $-\pi^+$. The corresponding propagation amplitude will be zero since the matrix element of the pion annihilating operator between the π^+ and vacuum states is zero. To demonstrate the translational invariance, we also show fitted pion masses, which were obtained after shifting the gauge configuration in t direction by 0, 8, 16, and 24 slices. The mass values are compatible with each other and also with the mass obtained from a lattice of same size with periodic boundary condition.

V. DISCUSSION AND OUTLOOK

The last sections show that a lot of properties of observables in the P -periodic setting are similar or better than those in the open setting where the field space is connected. In particular, the autocorrelation time of local quantities like the topological charge on a time slice improves to the level of open boundary conditions without showing boundary artifacts. However, this does not mean that the field space in the P -periodic setup is connected. This can be seen, for example, in the instanton picture. In the periodic case the topological sectors are labeled by the net number of instantons with positive and negative charge $N_+ - N_-$, which is an integer and conserved. The total instanton number $N_+ + N_-$ is only conserved $\text{mod } 2$ due to instanton pair creation and annihilation. For open lattices N_+ , N_- , and $N_+ \pm N_-$ are not well defined, so instantons do not lead to multiple sectors in field space. For the P -periodic case instantons can propagate once around the P -periodic direction and become anti-instantons, so N_+ ,

N_- , and $N_+ - N_-$ are also not well defined. However, the total instanton number $N_+ + N_-$ is conserved by this process and like on the torus is well defined (mod 2). This suggests there are still two sectors in field space which correspond to the even and odd sectors on the torus, and that the same lattice artifacts are necessary to move between these sectors. Then also the critical slowing down affects the tunneling rate identically as on the torus. But in the case with P -periodic boundary conditions, i.e. only two sectors, it is much simpler to simulate long enough such that all sectors are sampled well. Already this makes the simulation at smaller lattice spacings feasible.

Having only two sectors also opens up possibilities to study even smaller lattice spacings with completely frozen topology if the relative weight of the two sectors is known. This can be achieved, for example, by integrating up the relative weight of the two sectors starting at a coupling where there is still enough tunneling between the sectors. This strategy has recently been applied at high temperatures where there are only two sectors relevant as well [33,34]. P -periodic boundaries make this method applicable also at low temperatures where on the torus at reasonable volumes many sectors with different relative weights contribute.

In this article we have shown how to formulate and simulate lattice QCD on a nonorientable space-time manifold. For the pure gauge case our simulations show that this change in the topology of space-time leads to a strong reduction of the autocorrelation time of the topological charge density comparable to the improvement observed using open boundary conditions. While the pure gauge case is straightforward to construct and its implementation is virtually free of additional numerical cost, the inclusion of fermions is not trivial. We have demonstrated how to combine nonorientable space-time with charge conjugation or flavor symmetry to get a real fermionic contribution to the action and also how to measure fermionic observables. Testing the new boundaries for dynamical fermions is left for future work. It will be especially interesting to compare the numerical costs to that of e.g. open boundary conditions. Since it depends on the implementation details of fermions in the Majorana basis, we refrain from a precise cost estimation at this point.

ACKNOWLEDGMENTS

The authors thank Tamas Kovacs and Daniel Nogradi for discussions and useful comments on the manuscript. S.M. thanks Jakob Simeth, Florian Rapp, and Rudolf Rödl for many discussions on possible applications of nonorientable manifolds in particle physics. The simulations were performed on the GCS supercomputers JUQUEEN at JSC in Jülich, on SuperMUC at LRZ in Garching, and on the QPACE machines funded by the DFG Grant No. SFB/TR55.

APPENDIX: SYMMETRIES OF THE FERMION ACTION

In this appendix we list the symmetries of the single flavor fermion action in the Majorana representation, i.e. in the basis of eigenstates of the charge conjugation operation. For the definition see [20]. We use the following representation for the charge conjugation matrix: $C = i\gamma_5\gamma_t = C^\dagger = C^{-1} = -C^t$. The usual fermion action is

$$S_f[\psi, \bar{\psi}, U] = \bar{\psi} D[U] \psi.$$

Applying the following transformation,

$$\eta = \frac{1}{\sqrt{2}} \begin{pmatrix} 1 & C \\ -i & iC \end{pmatrix} \begin{pmatrix} \psi \\ \bar{\psi}^t \end{pmatrix},$$

we get

$$S_f[\eta, U] = -\frac{1}{2} \eta^t C \hat{D}[U] \eta,$$

where $\hat{D}[U] = D[\text{Re}U \cdot \mathbf{1}_{2 \times 2} - i \text{Im}U \cdot \rho_2]$.

1. Infinite volume

First, we start with the symmetries of the fermion action in infinite volume. The symmetries also apply in a finite box with periodic boundary conditions. The transformation for the gauge fields is standard and not shown explicitly.

(1) U(1) phase transformation:

$$\begin{aligned} \psi &\rightarrow \exp(i\theta)\psi & \bar{\psi} &\rightarrow \bar{\psi} \exp(-i\theta), \\ \eta &\rightarrow \exp(-i\theta\rho_2)\eta. \end{aligned}$$

(2) U(1) chiral transformation for a massless fermion in the continuum:

$$\begin{aligned} \psi &\rightarrow \exp(i\theta\gamma_5)\psi & \bar{\psi} &\rightarrow \bar{\psi} \exp(i\theta\gamma_5), \\ \eta &\rightarrow \exp(i\theta\gamma_5)\eta. \end{aligned}$$

(3) Charge conjugation:

$$\psi \rightarrow C\bar{\psi}^t \quad \text{and} \quad \bar{\psi} \rightarrow -\psi^t C, \quad \eta \rightarrow \rho_3\eta.$$

(4) Translations along the μ axis with $x'_\mu = x_\mu + 1$:

$$\psi(x) \rightarrow \psi(x') \quad \text{and} \quad \bar{\psi}(x) \rightarrow \bar{\psi}(x'), \quad \eta(x) \rightarrow \eta(x').$$

(5) μ -axis reversal with $x'_\mu = -x_\mu$:

$$\begin{aligned}\psi(x) &\rightarrow \gamma_5 \gamma_\mu \psi(x') \quad \text{and} \quad \bar{\psi}(x) \rightarrow \bar{\psi}(x') \gamma_\mu \gamma_5, \\ \eta(x) &\rightarrow -\gamma_5 \gamma_\mu \rho_2 \eta(x').\end{aligned}$$

(6) 90° rotation in $\mu\nu$ plane with $x'_\mu = -x_\nu, x'_\nu = x_\mu$:

$$\begin{aligned}\psi(x) &\rightarrow \exp\left(-i\frac{\pi}{2}\sigma_{\mu\nu}\right)\psi(x') \quad \text{and} \\ \bar{\psi}(x) &\rightarrow \bar{\psi}(x') \exp\left(i\frac{\pi}{2}\sigma_{\mu\nu}\right), \\ \eta(x) &\rightarrow \exp\left(-i\frac{\pi}{2}\sigma_{\mu\nu}\right)\eta(x'),\end{aligned}$$

$$\text{where } \sigma_{\mu\nu} = -\frac{i}{4}[\gamma_\mu, \gamma_\nu].$$

2. CP boundary

Here we list the symmetries of the theory with CP -boundary conditions. In the spatial directions we have usual periodic boundary conditions, whereas in the time direction we have

$$\begin{aligned}U_x(x, y, z, t + T) &= U_x^t(L - x - 1, y, z, t), \\ U_i(x, y, z, t + T) &= U_i^*(L - x, y, z, t), \quad i = y, z, t\end{aligned}$$

for the gauge fields and

$$\eta(x, y, z, t + T) = -\gamma_5 \gamma_x \rho_2 \rho_3 \eta(L - x, y, z, t)$$

for the fermions. The symmetries are

(1) Sign transformation:

$$\psi \rightarrow -\psi \quad \text{and} \quad \bar{\psi} \rightarrow -\bar{\psi}, \quad \eta \rightarrow -\eta.$$

(2) Combined chiral and $U(1)$ phase transformation for a massless fermion in the continuum:

$$\psi \rightarrow -\gamma_5 \psi \quad \text{and} \quad \bar{\psi} \rightarrow \bar{\psi} \gamma_5, \quad \eta \rightarrow \gamma_5 \rho_2 \eta.$$

(3) Charge conjugation combined with a $U(1)$ phase transformation:

$$\psi \rightarrow iC\bar{\psi}^t \quad \text{and} \quad \bar{\psi} \rightarrow i\psi^t C, \quad \eta \rightarrow -i\rho_2 \rho_3 \eta.$$

(4) Translations along the μ axis for $\mu = y, z, t$.

(5) μ -axis reversal for $\mu = y, z, t$.

μ -axis reversal combined with a $U(1)$ phase transformation for $\mu = x$:

$$\begin{aligned}\psi(x) &\rightarrow i\gamma_5 \gamma_\mu \psi(x') \quad \text{and} \quad \bar{\psi}(x) \rightarrow -i\bar{\psi}(x') \gamma_\mu \gamma_5, \\ \eta(x) &\rightarrow i\gamma_5 \gamma_\mu \eta(x').\end{aligned}$$

(6) 90° rotation in the yz plane.

-
- [1] P. van Baal, *Commun. Math. Phys.* **85**, 529 (1982).
[2] S. Schaefer, R. Sommer, and F. Virota (ALPHA Collaboration), *Nucl. Phys.* **B845**, 93 (2011).
[3] R. Brower *et al.* (LSD Collaboration), *Phys. Rev. D* **90**, 014503 (2014).
[4] M. Luscher and S. Schaefer, *J. High Energy Phys.* **07** (2011) 036.
[5] M. Luscher and S. Schaefer, *Comput. Phys. Commun.* **184**, 519 (2013).
[6] M. Bruno, P. Korcyl, T. Korzec, S. Lottini, and S. Schaefer, *Proc. Sci.*, LATTICE2014 (2014) 089 [arXiv:1411.5207].
[7] A. Amato, G. Bali, and B. Lucini, *Proc. Sci.*, LATTICE2015 (2015) 292 [arXiv:1512.00806].
[8] B. Lucini, C. McNeile, and AF. Rago, *Proc. Sci.*, LATTICE2015 (2015) 102 [arXiv:1511.09303].
[9] S. Aoki, H. Fukaya, S. Hashimoto, and T. Onogi, *Phys. Rev. D* **76**, 054508 (2007).
[10] W. Bietenholz, P. de Forcrand, and U. Gerber, *J. High Energy Phys.* **12** (2015) 070.
[11] I. Bautista, W. Bietenholz, A. Dromard, U. Gerber, L. Gonglach, C. P. Hofmann, H. Mejía-Díaz, and M. Wagner, *Phys. Rev. D* **92**, 114510 (2015).
[12] R. Brower, S. Chandrasekharan, J. W. Negele, and U. J. Wiese, *Phys. Lett. B* **560**, 64 (2003).
[13] R. Kitano and N. Yamada, *J. High Energy Phys.* **10** (2015) 136.
[14] A. Laio, G. Martinelli, and F. Sanfilippo, *J. High Energy Phys.* **07** (2016) 089.
[15] G. McGlynn and R. D. Mawhinney, *Proc. Sci.*, LATTICE2013 (2014) 027 [arXiv:1311.3695].
[16] M. G. Endres, R. C. Brower, W. Detmold, K. Orginos, and A. V. Pochinsky, *Phys. Rev. D* **92**, 114516 (2015).
[17] W. Detmold and M. G. Endres, *Phys. Rev. D* **94**, 114502 (2016).
[18] U. Wiese, *Nucl. Phys.* **B375**, 45 (1992).
[19] A. S. Kronfeld and U. J. Wiese, *Nucl. Phys.* **B357**, 521 (1991).
[20] B. Lucini, A. Patella, A. Ramos, and N. Tantalo, *J. High Energy Phys.* **02** (2016) 076.

- [21] M. Luscher and P. Weisz, *Phys. Lett.* **158B**, 250 (1985).
- [22] N. Cabibbo and E. Marinari, *Phys. Lett.* **119B**, 387 (1982).
- [23] A. D. Kennedy and B. J. Pendleton, *Phys. Lett.* **156B**, 393 (1985).
- [24] M. Creutz, *Phys. Rev. D* **36**, 515 (1987).
- [25] S. Borsanyi, S. Durr, Z. Fodor, C. Hoelbling, S. D. Katz *et al.*, *J. High Energy Phys.* **09** (2012) 010.
- [26] R. Sommer, *Proc. Sci.*, LATTICE2013 (2014) 015 [arXiv:1401.3270].
- [27] M. Lüscher, *J. High Energy Phys.* **08** (2010) 071; **03** (2014) 92.
- [28] G. McGlynn and R. D. Mawhinney, *Phys. Rev. D* **90**, 074502 (2014).
- [29] B. Grinstein and R. Rohm, *Commun. Math. Phys.* **111**, 667 (1987).
- [30] M. A. Metlitski, arXiv:1510.05663.
- [31] Z. Bai *et al.* (RBC, UKQCD Collaboration), *Phys. Rev. Lett.* **115**, 212001 (2015).
- [32] C. Morningstar and M. J. Peardon, *Phys. Rev. D* **69**, 054501 (2004).
- [33] S. Borsanyi *et al.*, *Nature (London)* **539**, 69 (2016).
- [34] J. Frison, R. Kitano, H. Matsufuru, S. Mori, and N. Yamada, *J. High Energy Phys.* **09** (2016) 021.